Journal of Electrical and Electronic Materials

View Online CrossMark

Early Stage Report: Graduate Research

Structural Stability and Electromechanical Response of Lead-Free $(Bi_{1/2}Na_{1/2})TiO_3$–$SrTiO_3$ Ceramics Under A-Site Strontium Non-Stoichiometry

Yubin Kang[1], Trang An Duong[1], Gwang-Hwi Jeong[1], Chang Won Ahn[2], Yong-Jai Kwon[1], Hyoung-Su Han[1]*

[1] School of Materials Science and Semiconductor Engineering, University of Ulsan, Ulsan 44776, Korea

[2] Quintess Co., Ltd., Uiwang 16108, Korea

Corresponding author(s): hsejs@ulsan.ac.kr. (H. S. Han)

Cite as J. Electr. Electron. Mater., 39(5), 549–555 (2026), DOI: https://doi.org/10.4313/JEEM.2026.39.5.12

Received July 8, 2026; Revised July 31, 2026; Accepted August 3, 2026

ABSTRACT: Lead-free $(Bi_{1/2}Na_{1/2})TiO_3$ (BNT)-based incipient piezoelectrics are highly promising for high strain actuators, but the high electric fields (4 ~ 6 kV/mm) required for activation limit practical device integration. In the current literature, large strains are frequently attributed to local structural variations like microscopic core-shell architectures. This work systematically investigates an alternative pathway by introducing A-site Strontium (Sr) excess non-stoichiometry into $0.74(Bi_{1/2}Na_{1/2})TiO_3$–$0.26SrTiO_3$ (BNST26) ceramics. Microstructural and X-ray diffraction analyses reveal highly dense, uniform matrices completely devoid of micro-scale core-shell boundaries or macroscopic symmetry distortions, revealing that Sr non-stoichiometry diverges from typical Bi-excess mechanisms. Interestingly, despite negligible variations in overall macro-scale strain behavior across the composition series, a peak normalized strain (S_{max}/E_{max}) of approximately 804 pm/V is achieved at a low driving field of 2 kV/mm for the 1 mol% Sr-excess specimen (x = 0.010). These results indicate that while Sr non-stoichiometry weakly influences nanoscale stability, it can be inferred that subtle modifications of local defect configurations optimize switching energy barriers, enabling high-strain, low-drive-field performance in lead-free relaxors.

KEYWORDS: Lead-free piezoceramics, A-site Sr-excess, Polar nanoregions (PNRs), Threshold electric field, Large electromechanical strain

The urgent global mandate to replace commercial lead-based piezoelectric ceramics, such as lead zirconate titanate ($Pb(Zr,Ti)O_3$; PZT), stems from severe environmental toxicity and the significant health hazards associated with lead volatilization during high-temperature processing [1-3]. Among various lead-free alternatives under intensive investigation, bismuth sodium titanate-based ($(Bi_{1/2}Na_{1/2})TiO_3$; BNT) ceramics have emerged as exceptionally promising candidates. These systems are highly celebrated for their abnormally large electromechanical strain capabilities, positioning them as prime candidates for next-generation actuating devices and precision positioning applications [4-6].

Despite their massive strain potential, the practical engineering integration of BNT-based ceramics remains restricted by a critical technological bottleneck. Specifically, excessively high threshold electric fields (≈ 4 ~ 6 kV/mm) are typically required to trigger their large electromechanical response. This massive field requirement stems from the energy barrier associated with forcing the material from an unpolarized state into a long-range ordered ferroelectric phase. Consequently, optimizing these “incipient” piezoelectrics [5-10] to lower the threshold operating fields while

maintaining giant unipolar strain performance remains the most critical hurdle facing contemporary relaxor ceramic research.

Recently, prominent advancements in the literature have highlighted chemical heterogeneity as a viable route to tune these threshold landscapes. Specifically, elegant work focusing on Bismuth (Bi) non-stoichiometry demonstrated that intentionally introducing an A-site Bi-excess can effectively suppress atomic diffusion during thermal sintering [11]. This controlled diffusion successfully "freezes" local chemical imbalances, establishing microscopic core-shell structures [11-14] that serve as a powerful structural strategy to stabilize giant electromechanical strains. Extending this conceptual framework to the strontium-modified BNT system, this study builds an exploratory design path to investigate whether intentionally introducing A-site Strontium (Sr) excess non-stoichiometry would act as a similar microstructural or phase-boundary lever to control electromechanical performance.

To systematically investigate this potential pathway, this work comprehensively evaluates the structural and electromechanical implications of intentional A-site Strontium (Sr) excess non-stoichiometry in lead-free $0.74(Bi_{1/2}Na_{1/2})TiO_3$–$0.26SrTiO_3$ (BNST26) ceramics. We evaluate the material's bulk sinterability through precise measurements of linear shrinkage and relative density. Furthermore, the evolution of crystal structures and surface micro-structures are tracked using X-ray diffraction (XRD) and field-emission scanning electron micros-copy (FE-SEM) to explicitly look for signs of phase purity and micro-scale structural variations. Finally, temperature-dependent dielectric spectra, ferroelectric polarization loops, and unipolar strain curves are analyzed to clarify the exact impact of Sr-excess on the electromechanical properties and field sensitivity of the BNST26 ceramics. Through this systematic approach, this study establishes a foundational baseline for understanding the boundary constraints of non-stoichiometric A-site engineering in lead-free relaxor ceramics.

Lead-free strontium-excessed bismuth sodium titanate-strontium titanate ceramic specimens, with the nominal composition of $0.74(Bi_{1/2}Na_{1/2})TiO_3$–$0.26(Sr_{1+x})TiO_3$ (abbreviated as Sr-excessed BNST26 ceramics or Sr1+x, where x = 0, 0.005, 0.010, and 0.015), were synthesized using a conventional solid-state reaction technique. Reagent-grade oxide and carbonate powders of Bi_2O_3 (99.99%), Na_2CO_3 (99.0%), TiO_2 (99.99%), and $SrCO_3$ (99.9%), all sourced from High Purity Chemicals, Japan, were utilized as the raw starting materials. These constituent powders were accurately weighed according to the stoichiometric proportions required for each composition. The weighed mixtures were ball-milled in an ethanol medium for 24 h using stabilized ZrO_2 grinding balls. The resulting wet slurries were subsequently dried in a drying oven at 100°C for 24 h.

Following complete drying, the powder aggregates were thoroughly crushed and calcined in a furnace inside covered alumina crucibles at 850°C for 2 h, using a constant heating rate of 5 °C/min. The calcined powders were subjected to a second 24 h ball-milling process in ethanol and dried under identical conditions. Polyvinyl alcohol (PVA) aqueous solution was then incorporated as a temporary binding agent during granulating. The granulated mixtures were uniaxially pressed into disk-shaped green compacts with a diameter of 12 mm under a molding pressure of 98 MPa. These green pellets were placed in covered alumina crucibles and sintered at 1,175°C for 2 h in ambient air, maintaining a heating rate of 5 °C/min.

Bulk sinterability was evaluated by tracking the linear shrinkage, and the experimental bulk densities of the sintered disks were determined using the Archimedes immersion method with an electronic densimeter (SD-120 L, A&D, Japan). The crystal structures and phase evolution were verified by an X-ray diffractometer (XRD, Ultima, Rigaku, Japan) over a 2θ range of 20° ~ 80°. Microstructural details were observed on polished and thermally etched cross-sections of the ceramic specimens via field-emission scanning electron microscopy (FE-SEM, JSM-6500F, JEOL, Japan).

For the electrical characterization, the sintered samples were systematically polished down to a parallel thickness of 1 mm. Conductive silver paste was screen-printed onto both parallel disk faces and baked at 700°C for 30 min to establish electroded surfaces. To verify the ferroelectric-to-relaxor transition behavior (T_{F-R}), selected samples were poled at room temperature in a silicone oil bath under a direct current (DC) field of 4 kV/mm for 15 min. Temperature- and frequency-dependent dielectric constant (ε_r) and dielectric loss (tanδ) profiles were recorded for both poled and unpoled samples over a wide frequency spectrum (1 ~ 100 kHz) using an automated high-temperature prober system connected to a Precision LCR Meter (E4980AL, Keysight, USA). Finally, the electric-field-induced polarization hysteresis (P–E) and bipolar/unipolar strain (S–E) curves were measured at a driving frequency of 1 Hz in a silicone oil bath using a modular aixACCT ferroelectric test system (aixPES, aixACCT, Germany).

Figure 1 illustrates the bulk sinterability indicators and the baseline room-temperature dielectric properties of the Sr1+x ceramics plotted against the nominal A-site Strontium excess concentration. As shown in Fig. 1(a), all ceramic specimens demonstrate excellent densification behavior, maintaining highly competitive linear shrinkage values between approximately 15% and 16% regardless of the shifting stoichiometry. Concurrently, the

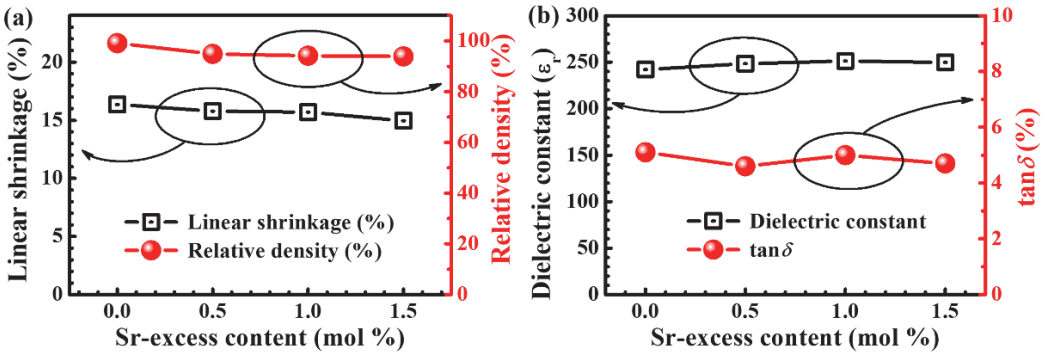

Fig. 1. (a) Sinterability behaviors (linear shrinkage and relative density) and (b) room-temperature dielectric properties (ε_r and tanδ) of Sr1+x ceramics as a function of Sr-excess content

calculated relative densities consistently exceed 94% across all compositions. A slight, monotonic decrease in bulk relative density is discernible, dropping from its peak value at x = 0 toward the highly modified x = 0.015 sample. However, all values remain well within the acceptable boundaries for dense bulk perovskite matrices [5]. This confirms that the selected sintering temperature of 1,175°C was highly appropriate.

Figure 1(b) displays the corresponding room-temperature dielectric constant (ε_r) and dielectric loss (tanδ) profiles evaluated as a function of the A-site Sr-excess content. Interestingly, the baseline dielectric constant shows an exceptionally stable trend, fluctuating narrowly around a value of ≈ 250 as the non-stoichiometry changes. This high degree of stability indicates that the structural integrity of the underlying perovskite lattice is well preserved, and that excess Strontium does not induce substantial macroscopic phase transformations at room temperature. Simultaneously, the dielectric loss remains steadily low and uniform, staying bounded between 4.6% and 5.1% across all samples. This consistently low tanδ behavior correlates well with the high relative density data from Fig. 1(a), verifying that the introduction of A-site Strontium excess does not generate highly mobile leakage paths or severe macro-scale degradation mechanisms within the BNST26 ceramics.

Figures 2(a) ~ (d) present the field-emission scanning electron microscopy (FE-SEM) images taken from the thermally etched surfaces of the Sr1+x specimens. Interestingly, the microstructural developments reveal a clear distinction from recent literature regarding A-site non-stoichiometry. While reports on Bismuth (Bi) excess frequently show the formation of distinct microscopic core-shell boundaries to stabilize strain [11-13], the introduction of A-site Strontium (Sr) excess exhibits a fundamentally different behavior. Across all levels of x, the ceramic matrices display a

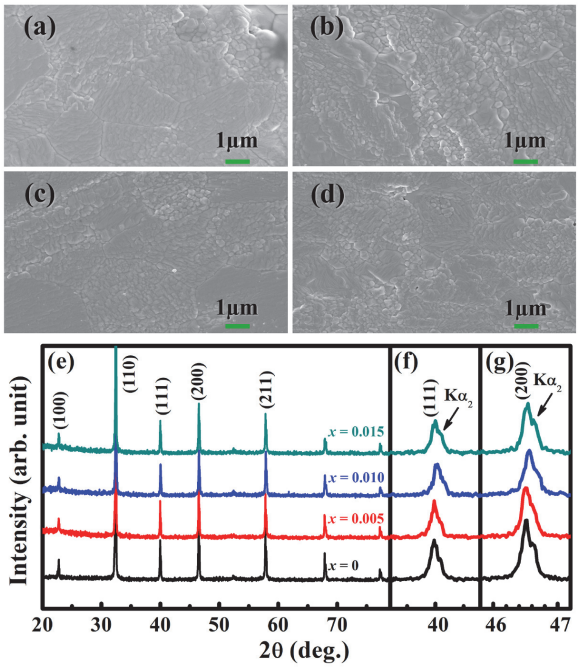

Fig. 2. Surface microstructures (top) and XRD patterns (bottom) of the Sr1+x ceramics as a function of Sr-excess content: (a) x = 0, (b) x = 0.005, (c) x = 0.010, (d) x = 0.015, and the corresponding 2θ range of (e) 20 ~ 80°, (f) ~ 40°, (g) 46 ~ 47°

visually uniform and clean morphology without any discernible micro-scale core-shell structural networks. Instead, a highly dense, well-sintered, and homogeneous grain distribution is stabilized across all compositions. This observation demonstrates that the structural pathway induced by Sr-excess non-stoichiometry diverges from the typical Bi-excess mechanism in this relaxor

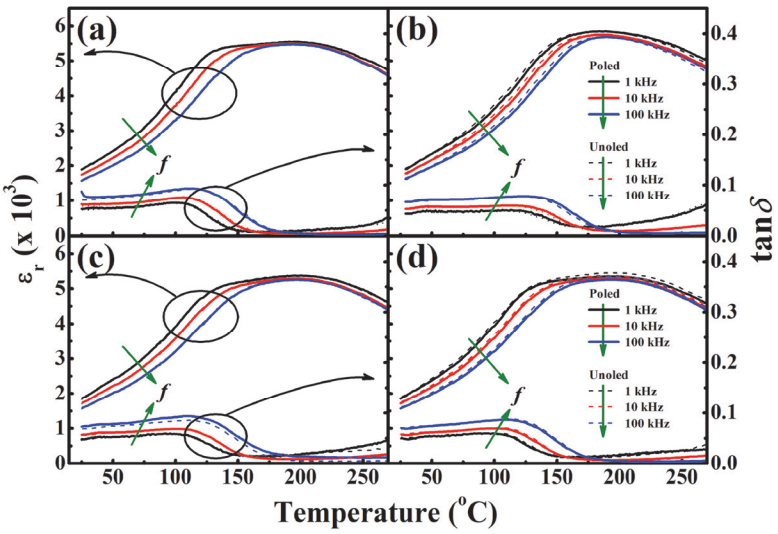

Fig. 3. Temperature-dependent dielectric constant (ε_r) and dielectric loss (tanδ) behaviors of poled (solid line) and unpoled (dashed line) Sr1-x ceramics at various frequencies (1, 10, and 100 kHz): (a) x = 0, (b) x = 0.005, (c) x = 0.010, and (d) x = 0.015

environment. Consequently, it indicates that the prominent low-field electromechanical responses obtained in this system originate from an alternative nanoscale mechanism rather than micro-scale boundary phase segregation.

To verify whether this structural uniformity and chemical homogeneity persist down to the lattice level, X-ray diffraction (XRD) analysis was performed. As shown in the X-ray diffractograms in Fig. 2(e), all compositions exhibit a pure single perovskite structure with no detectable traces of secondary or impurity phases. Detailed examinations of the selected 2θ regions around the (111) reflection at ≈ 40° (Fig. 2(f)) and the (200) reflection at around 46.5 (Fig. 2(g)) reveal highly symmetric, single peaks across all modified samples. No evidence of distinct peak splitting is observable, save for the standard Kα2 peaks. This behavior confirms a macroscopically (pseudo) cubic phase, showing that the solid solution structure remains stable without experiencing symmetry distortions or macro-scale phase segregation as the non-stoichiometry changes.

Figure 3 presents the temperature-dependent dielectric constant (ε_r) and dielectric loss (tanδ) behaviors of both poled and unpoled Sr1+x ceramics across a frequency range of 1 to 100 kHz. All compositions exhibit classic relaxor ferroelectric characteristics, marked by a broad, frequency-dispersive dielectric maximum (T_m) extending around 180 ~ 200 °C [5,7,8]. As indicated by the green arrows labeled f, increasing the measurement frequency results in a downward shift of ε_r and a corresponding upward shift in tanδ at lower temperatures. A critical observation is the near-perfect overlap between the curves of the poled (solid lines) and unpoled (dashed lines) specimens across the entire measured temperature range, even for the unmodified x = 0 specimen. In typical non-ergodic relaxor (NER) systems, electric-field poling induces a long-range, stable ferroelectric phase that destroys relaxor dispersion at room temperature, causing a massive mismatch between poled and unpoled dielectric behaviors below the ferroelectric to relaxor transition temperature (T_{F-R}) or the depolarization temperature (T_d) [8]. The absence of any discernable dielectric splitting or anomaly in Fig. 3 confirms that these Sr1+x ceramics were stabilized with dynamic ergodic relaxor (ER) state at room temperature. Because the field-induced ferroelectric phase immediately reverts back to the disordered ER state upon removing the electric field, the internal status of ceramics are dominated by highly mobile PNRs rather than deeply frozen macro-domains [7,8]. This fully supports our microstructural observations in Fig. 2. Without a frozen matrix or micro-scale core-shell boundaries to stabilize long-range order, the system maintains a highly sensitive free-energy boundary (ΔE), laying the exact physical foundation for low-field electromechanical strain activation [15].

To evaluate the impact of A-site Strontium excess on the electromechanical performance, the large-field polarization and strain responses were systematically measured at room temperature. As illustrated in Fig. 4(a), the polarization hysteresis (P-E) loops

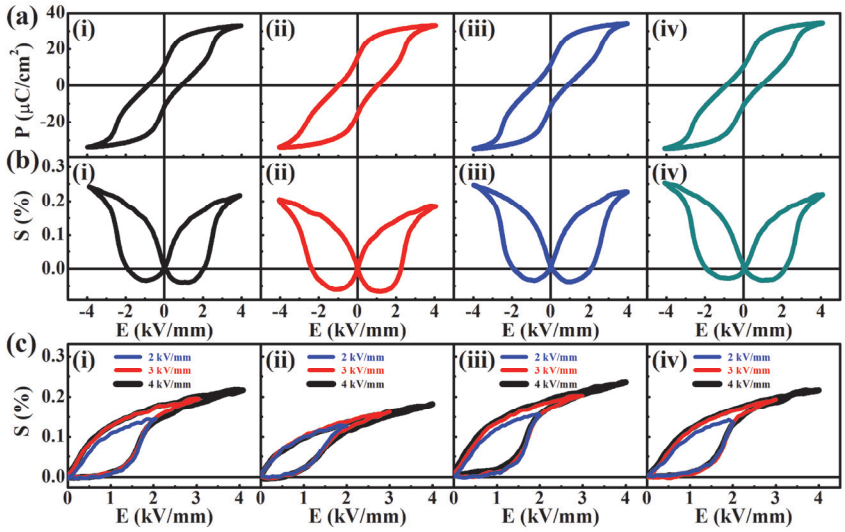

Fig. 4. (a) Electric-field-induced polarization (*P*-*E*) hysteresis loops, (b) bipolar strain (*S*-*E*) curves, and (c) unipolar strain (S-E) (under varying applied fields of 2 ~ 4 kV/mm) curves of Sr1-*x* ceramics: (i) $x = 0$, (ii) $x = 0.005$, (iii) $x = 0.010$, and (iv) $x = 0.015$

Table 1. Electromechanical properties (S_{max}, S_{max}/E_{max}, and d_{33}) of Sr1+*x* ceramics as a function of Sr-excess content

		S_{max} (%)			S_{max}/E_{max} (pm/V)			d_{33} (pC/N)
Applied electric field (kV/mm)		**2**	**3**	**4**	**2**	**3**	**4**	**4 (poling field)**
Sr content (mol %)	0	0.14	0.22	0.24	710	642	529	23
	0.5	0.13	0.16	0.20	641	545	456	25
	1.0	0.16	0.22	0.24	804	675	590	24
	1.5	0.15	0.22	0.25	732	646	543	23

under a driving field of 4 kV/mm exhibit pinched shapes with well-suppressed remanent polarization (P_r) values, while the corresponding bipolar strain (*S*-*E*) curves in Fig. 4(b) display a classic symmetric "sprout-like" geometry. These synchronized features confirm the complete dominance of a highly dynamic ergodic relaxor state across all compositions. Most notably, the unipolar strain (*S*-*E*) curves in Fig. 4(c) reveal nearly identical strain magnitudes and low-field activation characteristics regardless of the increasing Strontium excess concentration. Consequently, even though a drastic change in the overall strain behavior or the stabilized phase status is not revealed across the composition series, a maximum normalized strain (S_{max}/E_{max}) of approximately 804 pm/V is achieved at a low driving field of 2 kV/mm for the 1 mol% Sr-excess specimen ($x = 0.010$). When cross-referenced with the microstructural data in Fig. 2, this negligible variation in electromechanical performance provides a key physical insight. Because the excess Strontium does not influence the formation of microscopic core-shell structures or alter the local phase boundaries, it exerts a minimal footprint on the overall macroscopic strain output. Consequently, these results demonstrate that an A-site excess strategy using Strontium cannot replicate the structural or electromechanical tuning effects typically observed with Bismuth excess. This clear divergence highlights that the chemical nature of the A-site modifier is highly specific, meaning that Strontium non-stoichiometry weakly influences the nanoscale stability in the BNST26 system.

To understand how nominal Strontium non-stoichiometry is accommodated within the perovskite lattice without inducing core-shell structures or macro-scale phase transitions, the underlying defect chemistry and polar nanoregion (PNR) dynamics must be

considered. When nominal excess Sr^{2+} is incorporated into the A-site of the BNST26 matrix, lattice neutral balance is maintained primarily via the formation of A-site cation vacancies (V_A'', V_{Na}', or V_{Bi}'''), which can be expressed as:

$$2SrO \xrightarrow{\text{BNST matrix}} 2Sr_A^X + 2O_O^X + V_A'' \quad (1)$$

Unlike Bismuth-excess strategies that establish severe chemical gradients and microscopic core-shell structures, Strontium excess functions as a mild point-defect modifier within the ergodic relaxor matrix. At an optimal concentration of 1 mol% (x = 0.010), these localized A-site vacancies (V_A) and subtle ionic radii misfits (Sr^{2+} vs. Bi^{3+}/Na^+) can disrupt local elastic constraints around the dynamic PNRs. Therefore, it is suggested that this localized disorder flattens the internal free-energy landscape, lowering the energy barrier for field-induced PNR reorientation without altering the macroscopic cubic symmetry.

In summary, the structural and electromechanical implications of intentional A-site Strontium excess non-stoichiometry were systematically investigated in lead-free $0.74(Bi_{1/2}Na_{1/2})TiO_3$–$0.26SrTiO_3$ (BNST26) ceramics. X-ray diffraction and microstructural analyses revealed that the excess Strontium does not induce macro-scale phase segregation or the formation of microscopic core-shell structures, confirming a highly dense and structurally stable perovskite lattice. Correspondingly, large-field electromechanical measurements demonstrated that the characteristic ergodic relaxor state and overall unipolar strain curves remain remarkably uniform across the investigated composition series. Nevertheless, a peak normalized strain (S_{max}/E_{max}) of approximately 804 pm/V was successfully achieved under a low driving field of 2 kV/mm for the 1 mol% Sr-excess specimen (x = 0.010). This performance suggests that while Strontium non-stoichiometry only weakly affects the system's nanoscale stability, it likely optimizes the energy barriers for polar nanoregion (PNR) switching through local defect variations. These findings demonstrate a practical, low-field optimization pathway that works without needing micro-scale chemical heterogeneity, setting a clear boundary for non-stoichiometric engineering.

ORCID

Hyoung-Su Han https://orcid.org/0000-0002-7423-2862

Acknowledgement

This work was supported by the Technology Development Program (RS-2025-25303144) funded by the Ministry of SMEs and Startups (MSS, Korea).

Conflict of Interest

The authors (Chang Won Ahn, Hyoung-Su Han) currently serve on the editorial board of JEEM, but were not involved in any part of the publication process. Other than this, the authors declare that they have no relevant potential conflicts of interest.

Author Contributions

Yubin Kang: Methodology, Investigation, Resources, Data Curation, Visualization, Writing - Original Draft.
Trang An Duong: Validation, Formal analysis, Investigation, Data Curation.
Gwang-Hwi Jeong: Investigation, Resources, Data Curation.
Chang Won Ahn: Conceptualization, Data Curation, Visualization, Writing - Review & Editing.
Yong-Jai Kwon: Conceptualization, Methodology, Supervision, Writing - Review & Editing.
Hyoung-Su Han: Conceptualization, Methodology, Validation, Formal analysis, Supervision, Project administration, Funding acquisition, Writing - Original Draft, Writing - Review & Editing.

Data Availability

Data available on request from the authors

References

[1] C. H. Hong, H. P. Kim, B. Y. Choi, H. S. Han, J. S. Son, C. W. Ahn, and W. Jo, *J. Materiomics*, **2**, 1 (2016). doi: https://doi.org/10.1016/j.jmat.2015.12.002
[2] K. Zheng, N. Xie, Y. Deng, M. Febbo, C. Broeckmann, and P. Liu, *Chem. Eng. J.*, **528**, 172363 (2026). doi: https://doi.org/10.1016/j.cej.2025.172363
[3] T. A. Duong, F. Erkinov, M. Aripova, C. W. Ahn, B. W. Kim,

H. S. Han, and J. S. Lee, *Ceram. Int.*, **47**, 4925 (2021).
doi: https://doi.org/10.1016/j.ceramint.2020.10.066

[4] Z. Lv, H. Wang, Q. Qiu, W. Zhang, L. Luo, H. Tan, H. Zhang, L. Jin, A. Manan, G. Liu, and Y. Yan, *Ceram. Int.*, **52**, 23447 (2026).
doi: https://doi.org/10.1016/j.ceramint.2026.03.396

[5] Y. Kang, J. Y. Park, M. A. Devita, T. A. Duong, C. W. Ahn, B. W. Kim, H. S. Han, and J. S. Lee, *J. Korean Inst. Electr. Electron. Mater. Eng.*, **35**, 516 (2022).
doi: https://doi.org/10.4313/JKEM.2022.35.5.15

[6] E. S. Kang, S. J. Hyoung, Y. Kang, M. S. Park, T. A. Duong, J. S. Lee, and H. S. Han, *J. Korean Inst. Electr. Electron. Mater. Eng.*, **37**, 457 (2024).
doi: https://doi.org/10.4313/JKEM.2024.37.4.15

[7] W. Jo, R. Dittmer, M. Acosta, J. Zang, C. Groh, E. Sapper, K. Wang, and J. Rödel, *J. Electroceram.*, **29**, 71 (2012).
doi: https://doi.org/10.1007/s10832-012-9742-3

[8] H. S. Han, W. Jo, J. K. Kang, C. W. Ahn, I. W. Kim, K. K. Ahn, and J. S. Lee, *J. Appl. Phys.*, **113**, 154102 (2013).
doi: https://doi.org/10.1063/1.4801893

[9] Y. Lim, S. Pattipaka, H. Song, D. Kim, S. I. Jeong, Y. H. Son, S. Noh, M. Peddigari, J. Ryu, C. K. Jeong, and G. T. Hwang, *J. Korean Ceram. Soc.*, **63**, 381 (2026).
doi: https://doi.org/10.1007/s43207-025-00564-4

[10] Y. Lim and G. T. Hwang, *J. Electr. Electron. Mater.*, **39**, 225 (2026).
doi: https://doi.org/10.4313/JEEM.2026.39.3.1

[11] S. Bauer, M. Widenmeyer, and T. Frömling, *J. Eur. Ceram. Soc.*, **45**, 117588 (2025).
doi: https://doi.org/10.1016/j.jeurceramsoc.2025.117588

[12] J. Koruza, V. Rojas, L. Molina-Luna, U. Kunz, M. Duerrschnabel, H. J. Kleebe, and M. Acosta, *J. Eur. Ceram. Soc.*, **36**, 1009 (2016).
doi: https://doi.org/10.1016/j.jeurceramsoc.2015.11.046

[13] M. Acosta, L. A. Schmitt, L. Molina-Luna, M. C. Scherrer, M. Brilz, K. G. Webber, M. Deluca, H. J. Kleebe, J. Rödel, and W. Donner, *J. Am. Ceram. Soc.*, **98**, 3405 (2015).
doi: https://doi.org/10.1111/jace.13853

[14] S. Steiner, J. Heldt, O. Sobol, W. Unger, and T. Frömling, *J. Am. Ceram. Soc.*, **104**, 4341 (2021).
doi: https://doi.org/10.1111/jace.17845

[15] Y. Kang, V. N. Linh, T. A. Duong, C. W. Ahn, B. W. Kim, J. S. Lee, and H. S. Han, *J. Korean Ceram. Soc.*, **62**, 153 (2024).
doi: https://doi.org/10.1007/s43207-024-00451-4